

Nonlocal response of Mie-resonant dielectric particles

Daniel A. Bobylev,¹ Daria A. Smirnova,^{2,3} and Maxim A. Gorlach¹

¹*Physics and Engineering Department, ITMO University, Saint Petersburg 197101, Russia*

²*Nonlinear Physics Centre, Australian National University, Canberra ACT 2601, Australia*

³*Institute of Applied Physics, Russian Academy of Science, Nizhny Novgorod 603950, Russia*

Mie-resonant high-index dielectric particles are at the core of modern all-dielectric photonics. In many situations, their response to the external fields is well-captured by the dipole model, which incorporates electric and magnetic dipole moments of the scatterers neglecting higher-order multipole contributions. In that case, it is commonly assumed that the dipole moments induced by the external fields are given by the product of particle polarizability tensor and the field in the particle center. Here, we demonstrate that the dipole response of non-spherical subwavelength dielectric particles appears to be essentially more complex since the dipole moments are defined not only by the field in the particle center but also by the second-order *spatial derivatives of the field* thus giving rise to the nonlocal response of the individual scatterer which is especially pronounced in the vicinity of anapole minimum in the scattering cross-section. As an illustrative example, we examine the response of high-index dielectric disks applying group-theoretical analysis and retrieving the nonlocal corrections to the dipole response from full-wave numerical simulations. These results provide important insights into meta-optics of Mie-resonant non-spherical particles as well as metamaterials and metadevices based on them.

I. INTRODUCTION

Over the recent years, all-dielectric nanophotonics and meta-optics [1 and 2] have demonstrated a variety of exciting functionalities including the strong directional scattering of light [3 and 4], flexible phase manipulation of the transmitted signal with transparent metasurfaces [5], high-quality modes of dielectric particles [6], enhanced nonlinear phenomena in the arrays of resonant nanoparticles [7 and 8] and precise molecular fingerprinting with all-dielectric metasurfaces [9]. The physics underlying this plethora of effects is based on the combination of electric and magnetic responses of dielectric particles [10–12], where an optical magnetic response is associated with circular displacement currents excited in the scatterer.

A key theoretical tool to capture electromagnetic behavior of subwavelength objects is multipole expansion [13] which presents the field scattered by the particle as a sum of different multipoles, each of them being characterized by the unique set of polarization and angular dependence of the radiation pattern. In many situations, the dominant contribution to the scattering cross-section of subwavelength particles is provided by the lowest-order multipoles, namely, magnetic and electric dipoles, while the contribution of higher-order multipoles can be neglected.

In that case, the physics of complex particle arrays can be efficiently explored using the discrete dipole model [14–17]. In this approach, the scatterer is viewed as electric and magnetic dipoles placed in its center, while all information on particle properties is embedded into its electric and magnetic polarizability tensors. These tensors link the external fields acting on the particle to its dipole moments and can be retrieved from full-wave numerical simulations.

However, dielectric particles used in experimentally

relevant situations are not that deeply subwavelength, and the diameter of the particle has typically the same order of magnitude as the wavelength of light at magnetic or electric dipole resonance [2]. Therefore, it is not obvious *a priori* that electric and magnetic dipole moments of an arbitrarily shaped particle are related only to the field in the particle center, but do not depend on spatial derivatives of the field.

While the discussed physics is universally valid across the entire electromagnetic spectrum, in this Article we focus on the particles made of high-permittivity ceramics available in the microwave domain. We investigate the response of subwavelength high-index dielectric disks, when the choice of the particle center is straightforward, studying the frequency range where electric and magnetic dipole responses provide the dominant contribution to the scattering cross-section such that the contribution from the rest of multipoles is below 8%. Still, even under these circumstances, we reveal that the dipole moments of the disk are governed not only by electric and magnetic fields in its center but also by the second-order spatial derivatives of the fields which crucially determine the electromagnetic response of the disk in the vicinity of anapole minimum [18] in the scattering cross-section.

It should be stressed that our results are conceptually different from the nonlocal effects in small metallic nanoparticles manifested via size-dependent resonance shifts and linewidth broadening [19 and 20]. The latter effects occurring due to electron-electron interactions are enhanced as the size of plasmonic nanoparticle decreases. In stark contrast, the mechanism we discuss here becomes increasingly important as the size of the particle increases becoming of the same order of magnitude as the wavelength at the dipole resonance.

The rest of the article is organized as follows. In Sec. II we construct a general relation between the dipole moment of the particle from one side and incident field

with its spatial derivatives from the other using the symmetry arguments. To support our analysis further, in Sec. III we consider a dielectric particle made of high-permittivity ceramics. The parameters of the particle are chosen in such a way that the dipole response dominates the rest of multipole contributions in a sufficiently wide frequency range. Performing full-wave numerical simulations, we extract polarizability of the particle at the fixed frequency along with the nonlocal corrections to its dipole response. Finally, Sec. IV concludes with a summary and an outlook for future studies.

II. SYMMETRY ANALYSIS OF THE DISK RESPONSE

In the most general scenario, electric and magnetic dipole moments \mathbf{d} and \mathbf{m} of the particle induced by the impinging plane wave can be presented as Taylor series with respect to wave vector \mathbf{k} :

$$d_i = \varepsilon_0 \{ \alpha_{ij} E_j + \beta_{ijl} E_j k_l + \gamma_{ijlm} E_j k_l k_m + \dots \}, \quad (1)$$

$$m_i = \alpha_{ij}^{(m)} H_j + \beta_{ijl}^{(m)} H_j k_l + \gamma_{ijlm}^{(m)} H_j k_l k_m + \dots, \quad (2)$$

where SI system of units and $e^{-i\omega t}$ time convention are used. n^{th} terms of both expansions scale as $(R/\lambda)^n$ relative to the respective leading-order terms, where R is the particle characteristic size and λ is the wavelength. Therefore, assuming that the particle is subwavelength, we keep only the first three terms in Eqs. (1), (2).

Note that in the analysis below we define the dipole moment based on the angular dependence of the fields, consistently with Refs. [21 and 22]. In the alternative formulations of multipole expansion [23 and 24], however, thus defined d_i and m_i correspond to the sum of dipole moment, toroidal moment and higher-frequency contributions.

Tensors β_{ijl} and $\beta_{ijl}^{(m)}$ describe bianisotropic response of the particle being zero for any inversion-symmetric configuration including the case of the disk. Furthermore, $D_{\infty h}$ symmetry group of the disk ensures that the tensors α_{ij} , $\alpha_{ij}^{(m)}$ and γ_{ijlm} , $\gamma_{ijlm}^{(m)}$ have two and six independent components, respectively, which strongly simplifies the analysis (see the details in Appendix). Due to symmetry, these tensors can be constructed only from Kronecker symbols δ_{ij} and even powers of \mathbf{n} vector directed along the disk axis. Besides that, α_{ij} and γ_{ijlm} are symmetric with respect to the first pair (i, j) of the indices due to symmetry of kinetic coefficients [25]; γ_{ijlm} is also symmetric with respect to the last pair (l, m) of the indices. The above requirements yield:

$$\alpha_{ij} = \alpha_1 \delta_{ij} + \alpha_2 n_i n_j, \quad (3)$$

$$\begin{aligned} \gamma_{ijlm} = & \gamma_1 \delta_{ij} n_l n_m + \gamma_2 (n_i n_l \delta_{jm} + n_j n_m \delta_{il} \\ & + n_j n_l \delta_{im} + n_i n_m \delta_{jl}) + \gamma_3 n_i n_j n_l n_m \\ & + \gamma_4 \delta_{ij} \delta_{lm} + \gamma_5 (\delta_{il} \delta_{jm} + \delta_{im} \delta_{jl}) + \gamma_6 n_i n_j \delta_{lm}, \end{aligned} \quad (4)$$

where $\alpha_{1,2}$ and γ_{1-6} are some unknown scalar coefficients.

Combining Eqs. (3), (4) with Eqs. (1), (2), we derive the expression for the dipole moment of the disk:

$$\begin{aligned} d_i = & \alpha_{\perp} \varepsilon_0 E_i + (\alpha_{\parallel} - \alpha_{\perp}) n_i \varepsilon_0 E_z + \gamma_1 \varepsilon_0 E_i k_z^2 \\ & + 2\gamma_2 k_i k_z \varepsilon_0 E_z + \gamma_3 n_i \varepsilon_0 E_z k_z^2, \end{aligned} \quad (5)$$

where we take into account that $|\mathbf{k}| = k_0 = \omega/c$ and $\mathbf{k} \cdot \mathbf{E} = 0$ since the incident field satisfies the condition $\text{div } \mathbf{E} = 0$. α_{\perp} and α_{\parallel} are the standard frequency-dependent components of polarizability tensor of an anisotropic particle defined as $\alpha_{\perp} = \alpha_1 + \gamma_4 k_0^2$ and $\alpha_{\parallel} = \alpha_{\perp} + \alpha_2 + \gamma_6 k_0^2$. Similar equation holds for the magnetic dipole moment:

$$\begin{aligned} m_i = & \alpha_{\perp}^{(m)} H_i + (\alpha_{\parallel}^{(m)} - \alpha_{\perp}^{(m)}) n_i H_z + \gamma_1^{(m)} H_i k_z^2 \\ & + 2\gamma_2^{(m)} k_i k_z H_z + \gamma_3^{(m)} n_i H_z k_z^2. \end{aligned} \quad (6)$$

Quite importantly, if the particle is spherical and has full rotational symmetry, the only nonzero components of the tensors Eqs. (3), (4) are α_1 , γ_4 and γ_5 , which ensures that the link between the dipole moment and the field remains local.

In the case of a disk, second-order nonlocal corrections to the dipole moment of the particle are captured by the three additional terms proportional to γ_1 , γ_2 and γ_3 . Note that all of them exhibit characteristic dependence on the direction of the incident wave propagation since they depend on k_z . Based on this observation, we consider the geometry illustrated in Fig. 1.

TE-polarized wave [Fig. 1(a)] excites d_y , m_x and m_z

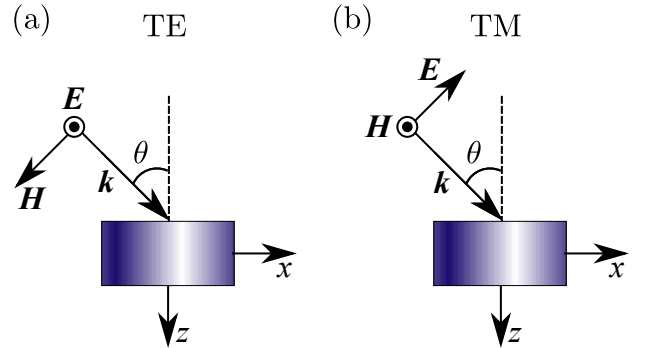


FIG. 1. Excitation of the disk by the incident plane wave. (a) TE-polarized excitation which induces d_y , m_x and m_z components of dipole moments; (b) TM-polarized excitation which induces d_x , d_z and m_y components of dipole moments.

components of the dipole moments given by the equations

$$d_y = (\alpha_{\perp} + \gamma_1 k_0^2 \cos^2 \theta) \varepsilon_0 E_0, \quad (7)$$

$$m_x = - \left\{ \left(\alpha_{\perp}^{(m)} - 2\gamma_2^{(m)} k_0^2 \right) \cos \theta + \left(\gamma_1^{(m)} + 2\gamma_2^{(m)} \right) k_0^2 \cos^3 \theta \right\} H_0, \quad (8)$$

$$m_z = \left\{ \left[\alpha_{\parallel}^{(m)} + \left(\gamma_1^{(m)} + 2\gamma_2^{(m)} + \gamma_3^{(m)} \right) k_0^2 \right] \sin \theta - \left(\gamma_1^{(m)} + 2\gamma_2^{(m)} + \gamma_3^{(m)} \right) k_0^2 \sin^3 \theta \right\} H_0, \quad (9)$$

whereas TM-polarized excitation [Fig. 1(b)] results in d_x , d_z and m_y components of the dipole moments:

$$m_y = \left(\alpha_{\perp}^{(m)} + \gamma_1^{(m)} k_0^2 \cos^2 \theta \right) H_0, \quad (10)$$

$$d_x = \left\{ \left(\alpha_{\perp} - 2\gamma_2 k_0^2 \right) \cos \theta + \left(\gamma_1 + 2\gamma_2 \right) k_0^2 \cos^3 \theta \right\} \varepsilon_0 E_0, \quad (11)$$

$$d_z = \left\{ - \left[\alpha_{\parallel} + \left(\gamma_1 + 2\gamma_2 + \gamma_3 \right) k_0^2 \right] \sin \theta + \left(\gamma_1 + 2\gamma_2 + \gamma_3 \right) k_0^2 \sin^3 \theta \right\} \varepsilon_0 E_0. \quad (12)$$

Hence, all relevant coefficients can be extracted by fitting the dependence of dipole moments on the incidence angle θ of the plane wave.

III. NUMERICAL SIMULATIONS

As a specific realization of cylindrical particles, we consider the disks made of high-permittivity ceramics $\varepsilon = 39$ with radius $R = 14.55$ mm and height $h = 11.61$ mm. Chosen parameters ensure that electric and magnetic dipole resonances residing in the range $f = (2.2 \div 2.8)$ GHz are well-separated from the higher-order multipole resonances. Furthermore, $2R/\lambda \approx 0.24$ in the chosen frequency range, which means that the size of the disk is of the same order of magnitude as the wavelength.

Examining the response of the disks to the incident TE-polarized plane wave [geometry Fig. 1(a), $\theta = \pi/2$], we recover a single characteristic peak in the scattering cross-section at frequencies around 2.4 GHz [Fig. 2(a)]. Multipole analysis of the scattered field reveals the dominant contribution of an electric dipole, while the contributions from magnetic dipole and from higher-order multipoles are strongly suppressed, which means that the incident field excites in-plane electric dipole resonance of the disk. Note also that the scattering spectrum has a pronounced minimum at frequencies around 2.5 GHz, which corresponds to the so-called anapole.

TM-polarized excitation [geometry Fig. 1(b), $\theta = \pi/2$] gives rise to the two scattering peaks: one around 2.4 GHz with the dominant contribution of in-plane magnetic dipole and another around 2.8 GHz, corresponding to z -oriented electric dipole. The contribution of higher-order multipoles to the scattering cross-section in the frequency range $(2.20 \div 2.75)$ GHz is below 4 cm^2 and

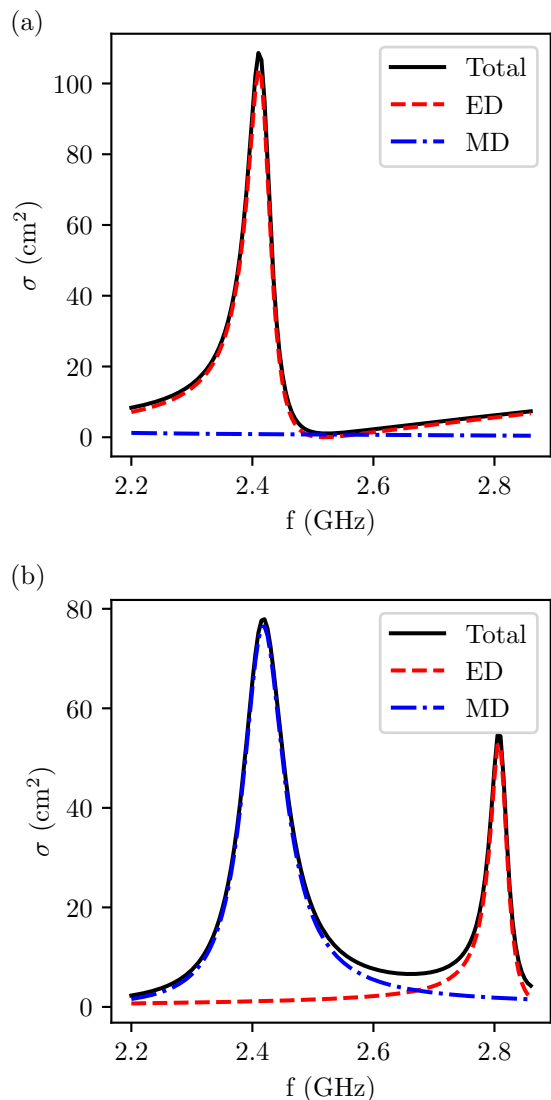


FIG. 2. Scattering spectrum of ceramic disk illuminated by the plane wave propagating along x axis. Solid line shows the total scattering cross-section, red dashed and blue dot-dashed curves show the contribution of electric and magnetic dipole moments, respectively. (a) TE-polarized plane wave with electric field along y axis. (b) TM-polarized plane wave with electric field along z axis.

0.25 cm^2 for TE- and TM-polarized excitations, respectively. Hence, the dipole model is clearly adequate in our case.

Next, we fix the frequency of excitation to be quite close to the anapole minimum, $f = 2.44$ GHz, varying the incidence angle θ . Using multipole decomposition technique [21–23], we evaluate complex amplitudes of the disk dipole moments for both polarizations of excitation as a function of θ . Setting the phase of the incident wave to zero in the disk center, we plot the results for TE and TM polarizations in Figs. 3 and 4, respectively.

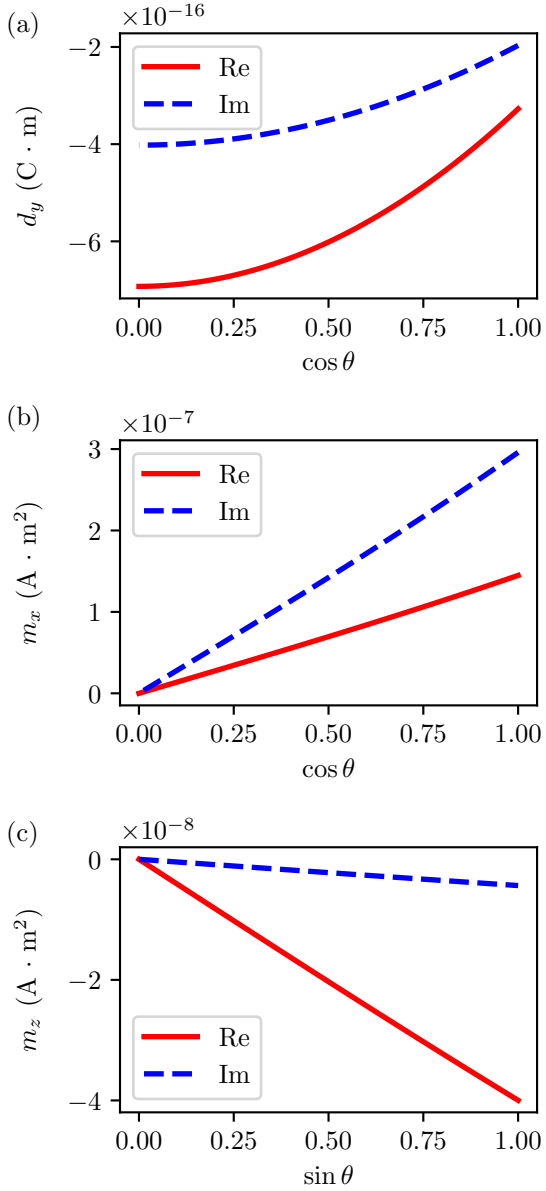


FIG. 3. Real and imaginary parts of dipole moments induced by the incident TE-polarized plane wave as a function of the incidence angle θ . (a) Electric dipole, y -component. (b) Magnetic dipole, x -component. (c) Magnetic dipole, z -component.

Interestingly, dipole moment d_y induced by TE-polarized plane wave features strong dependence on the incidence angle shown in Fig. 3(a). Since the disk is non-bianisotropic, this dipole moment occurs purely due to the electric field \mathbf{E} . However, y projection of the electric field does not depend on the incidence angle θ and therefore the results of simulations clearly show that the response of the disk is indeed beyond the simplified model based on local polarizability tensors. Somewhat similar situation is observed for TM-polarized excitation,

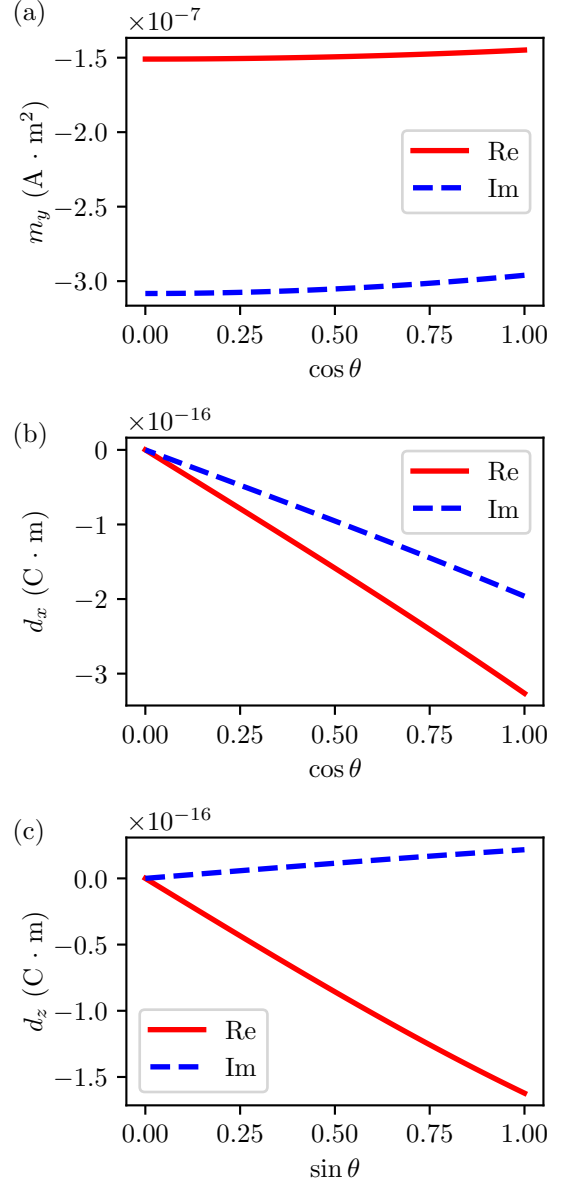


FIG. 4. Real and imaginary parts of dipole moments induced by the incident TM-polarized plane wave as a function of the incidence angle θ . (a) Magnetic dipole, y -component. (b) Electric dipole, x -component. (c) Electric dipole, z -component.

when induced magnetic moment m_y also depends on the incidence angle [Fig. 4(a)], serving as a fingerprint of “magnetic” nonlocalities. The rest of dipole moments [Fig. 3(b,c), Fig. 4(b,c)] feature almost linear dependence on $\cos \theta$ or $\sin \theta$ with relatively small deviations in agreement with Eqs. (8), (9), (11), (12).

To provide a more comprehensive picture, we fit the simulation data by Eqs. (7)-(12), extracting the relevant parameters: 5 for electric and 5 for magnetic dipole response of the disk. Calculated results are presented in

TABLE I. Polarizabilities and non-local parameters (SI)

Parameter	Electric response	Magnetic response
α_{\perp} , cm ³	$-78.3 + 45.4 i$	$-56.9 + 116.0 i$
α_{\parallel} , cm ³	$18.3 + 2.5 i$	$-15.1 + 1.6 i$
γ_4 , cm ⁵	$158 - 89 i$	$8.7 - 17.7 i$
γ_5 , cm ⁵	$-81.9 + 46.1 i$	$-9.8 + 19.8 i$
γ_6 , cm ⁵	$10.6 - 2.5 i$	$9.5 - 21.7 i$

Table I.

Chosen frequency close to the resonance for in-plane magnetic dipoles gives rise to a quite large imaginary part of magnetic polarizability $\alpha_{\perp}^{(m)}$. Real parts of polarizabilities $\alpha_{\parallel}^{(m)}$, $\alpha_{\perp}^{(m)}$ and $\alpha_{\perp}^{(m)}$ appear to be negative, since the considered frequency 2.44 GHz is higher than the resonance frequencies for z -oriented magnetic dipole or in-plane dipoles. At the same time, the frequency of excitation is below resonance frequency for z -oriented electric dipole, which ensures that the real part of α_{\parallel} is positive.

While conventional electric and magnetic polarizabilities have comparable magnitudes, “electric” nonlocal coefficients strongly exceed their “magnetic” counterparts. We associate such behavior with the choice of excitation frequency which appears to be quite close to the anapole minimum in the scattering spectrum. As a result, local electric polarizabilities are dramatically suppressed and nonlocal contributions become sizeable. Similarly, realizing the so-called magnetic anapole by canceling the radiation from the magnetic dipole, one can expect to substantially enhance magnetic nonlocalities.

IV. DISCUSSION AND OUTLOOK

In summary, we have investigated dipole response of Mie-resonant non-spherical particles in the region of crossover from $R/\lambda \ll 1$ to $R/\lambda \sim 1$, which is the case for experimentally relevant situations. As we have proved for the case of dielectric disks, dipole moments induced by the incident field are determined not only by the field in the particle center but also by the second-order spatial derivatives of the field, which gives rise to nonlocality of the particle dipole response. We have also demonstrated that the predicted nonlocal effects are especially pronounced in the vicinity of anapole minimum in the scattering spectrum reaching up to 50% of local response thereby largely governing light scattering in this frequency range.

Even though our simulations refer to the scenario of plane wave excitation, the obtained results including Eqs. (5), (6) for the dipole moments are easily generalized to the case of arbitrary spatial dependence of the fields by replacing k_n by $-i \partial_n$.

Furthermore, our results can be applied not only in the

microwave domain but also at infrared and visible frequencies, for instance, to silicon nanodisks, which have been studied extensively during the recent years [3 and 4]. In that case, however, higher-order multipole contributions have to be taken into account on the same footing with the nonlocal contributions to dipole moments, since dipole and higher-order multipole resonances are no longer well-separated due to lower refractive index.

The approach developed here can be directly generalized to the cases of less symmetric particles or larger scatterers when higher-order spatial derivatives of the field have to be incorporated. Moreover, our analysis can also be applied to the case of higher-order multipole moments, for instance, electric and magnetic quadrupoles. The nonlocal response of the individual scatterers provides an interesting perspective on spatial dispersion effects in metamaterials, which have previously been linked purely to the interactions of resonant scatterers with each other, while nonlocalities inherent to the individual meta-atoms were neglected [26–28].

Finally, we believe that our findings provide valuable insights into meta-optics and all-dielectric nanophotonics by highlighting truly nonlocal behavior of their basic building blocks — Mie-resonant nanoparticles.

ACKNOWLEDGMENTS

We acknowledge Pavel Belov for valuable discussions. Theoretical models were supported by the Russian Science Foundation (Grant No. 16-19-10538), numerical simulations were supported by the Russian Foundation for Basic Research (Grant No. 18-32-20065). M.A.G. acknowledges partial support by the Foundation for the Advancement of Theoretical Physics and Mathematics “Basis”.

APPENDIX. SYMMETRY ANALYSIS OF THE DISK DIPOLE RESPONSE

In this Appendix, we calculate the number of independent components of the tensors α_{ij} and γ_{ijklm} that enter Eq. (1) applying group-theoretical arguments [29]. We assume $D_{\infty h}$ symmetry group of the particle and take into account symmetry of the tensors with respect to permutation of i, j and l, m indices.

First, we notice that the vectors \mathbf{d} , \mathbf{E} and \mathbf{k} transform according to $E_{1u}(\Pi_u)$ representation of $D_{\infty h}$ symmetry group. To simplify our analysis, we consider finite D_{Nh} group setting $N \rightarrow \infty$ at later steps. This group includes rotations around vertical z axis by angles $\varphi_n = 2\pi n/N$, where $n = 0 \dots (N-1)$, further denoted as C_{φ} ; rotations by π around N horizontal symmetry axes of polygon, C'_2 ; all previous symmetry transformations followed by spatial inversion, iC_{φ} and iC'_2 . Note that identity element is contained in C_{φ} with $\varphi = 0$. The characters of all these

transformations for $E_{1u}(\Pi_u)$ representation are provided in the third line of the table II.

Without additional constraints, representations of the tensors α_{ij} and γ_{ijlm} correspond to the tensor products $\mathcal{D} \otimes \mathcal{D}$ and $\mathcal{D} \otimes \mathcal{D} \otimes \mathcal{D} \otimes \mathcal{D}$, respectively, where \mathcal{D} matrices realize $E_{1u}(\Pi_u)$ representation of D_{Nh} symmetry group. However, constructed matrix representations should also be symmetric with respect to the interchange of indices i, j and l, m . Hence, we should construct symmetrized matrices of representation

$$\bar{\mathcal{D}}_{ij,i'j'}(R) = \frac{1}{2} [\mathcal{D}_{ii'} \mathcal{D}_{jj'} + \mathcal{D}_{ij'} \mathcal{D}_{ji'}], \quad (13)$$

$$\begin{aligned} & \bar{\mathcal{D}}_{ijlm,i'j'l'm'}(R) \\ = & \frac{1}{4} [\mathcal{D}_{ii'} \mathcal{D}_{jj'} \mathcal{D}_{ll'} \mathcal{D}_{mm'} + \mathcal{D}_{ij'} \mathcal{D}_{ji'} \mathcal{D}_{ll'} \mathcal{D}_{mm'} \\ & + \mathcal{D}_{ii'} \mathcal{D}_{jj'} \mathcal{D}_{lm'} \mathcal{D}_{ml'} + \mathcal{D}_{ij'} \mathcal{D}_{ji'} \mathcal{D}_{lm'} \mathcal{D}_{ml'}]. \end{aligned} \quad (14)$$

The respective characters of these symmetrized representations are calculated as:

$$\bar{\chi}(R) = \frac{1}{2} [\chi^2(R) + \chi(R^2)], \quad (15)$$

$$\tilde{\chi}(R) = \frac{1}{4} [\chi^4(R) + 2\chi^2(R)\chi(R^2) + \chi^2(R^2)]. \quad (16)$$

Clearly, $\bar{\chi}$ and $\tilde{\chi}$ calculated for C_φ and iC_φ depend on φ , but in our analysis we are interested in the values of these

characters averaged over φ ; these values are provided in the fifth and sixth lines of the table II.

Finally, we can determine the number of independent components of the tensors under consideration by calculating the number of times that unity representation enters the constructed symmetrized representations:

$$\nu(\alpha) = \frac{1}{4N} \sum N_k \bar{\chi}(C_k) = 2, \quad (17)$$

$$\nu(\gamma) = \frac{1}{4N} \sum N_k \tilde{\chi}(C_k) = 6. \quad (18)$$

Hence, α_{ij} and γ_{ijlm} tensors contain two and six independent components, respectively, as indicated in the article main text.

TABLE II. Character table for $E_{1u}(\Pi_u)$ representation of D_{Nh} symmetry group in 3D case

R	C_φ	C'_2	iC_φ	iC'_2
N_k	N	N	N	N
$\chi(R)$	$1 + 2 \cos \varphi$	-1	$-1 - 2 \cos \varphi$	1
$\chi(R^2)$	$1 + 2 \cos 2\varphi$	3	$1 + 2 \cos 2\varphi$	3
$\langle \bar{\chi}(R) \rangle_\varphi$	2	2	2	2
$\langle \tilde{\chi}(R) \rangle_\varphi$	8	4	8	4

¹ A. I. Kuznetsov, A. E. Miroshnichenko, M. L. Brongersma, Y. S. Kivshar, and B. Luk'yanchuk, Optically resonant dielectric nanostructures, *Science* **354**, aag2472 (2016).

² S. Kruk and Y. Kivshar, Functional Meta-Optics and Nanophotonics Governed by Mie Resonances, *ACS Photonics* **4**, 2638 (2017).

³ I. Staude, A. E. Miroshnichenko, M. Decker, N. T. Fofang, S. Liu, E. Gonzales, J. Dominguez, T. S. Luk, D. N. Neshev, I. Brener, and Y. Kivshar, Tailoring Directional Scattering through Magnetic and Electric Resonances in Subwavelength Silicon Nanodisks, *ACS Nano* **7**, 7824 (2013).

⁴ M. Decker, I. Staude, M. Falkner, J. Dominguez, D. N. Neshev, I. Brener, T. Pertsch, and Y. S. Kivshar, High-Efficiency Dielectric Huygens' Surfaces, *Adv. Opt. Mater.* **3**, 813 (2015).

⁵ S. Kruk, B. Hopkins, I. I. Kravchenko, A. Miroshnichenko, D. N. Neshev, and Y. S. Kivshar, Broadband highly efficient dielectric metadevices for polarization control, *APL Photonics* **1**, 030801 (2016).

⁶ M. V. Rybin, K. L. Koshelev, Z. F. Sadrieva, K. B. Samusev, A. A. Bogdanov, M. F. Limonov, and Y. S. Kivshar, High- Q Supercavity Modes in Subwavelength Dielectric Resonators, *Phys. Rev. Lett.* **119**, 243901 (2017).

⁷ M. R. Shcherbakov, D. N. Neshev, B. Hopkins, A. S. Shorokhov, I. Staude, E. V. Melik-Gaykazyan, M. Decker, A. A. Ezhov, A. E. Miroshnichenko, I. Brener, A. A. Fedyanin, and Y. S. Kivshar, Enhanced Third-Harmonic Generation in Silicon Nanoparticles Driven by Magnetic Response, *Nano Lett.* **14**, 6488 (2014).

⁸ K. Koshelev, S. Kruk, E. Melik-Gaykazyan, J.-H. Choi, A. Bogdanov, H.-G. Park, and Y. Kivshar, Subwavelength dielectric resonators for nonlinear nanophotonics, *Science* **367**, 288 (2020).

⁹ A. Tittl, A. Leitis, M. Liu, F. Yesilkoy, D.-Y. Choi, D. N. Neshev, Y. S. Kivshar, and H. Altug, Imaging-based molecular barcoding with pixelated dielectric metasurfaces, *Science* **360**, 1105 (2018).

¹⁰ A. B. Evlyukhin, S. M. Novikov, U. Zywietz, R. L. Erikson, C. Reinhardt, S. I. Bozhevolnyi, and B. N. Chichkov, Demonstration of Magnetic Dipole Resonances of Dielectric Nanospheres in the Visible Region, *Nano Lett.* **12**, 3749 (2012).

¹¹ A. I. Kuznetsov, A. E. Miroshnichenko, Y. H. Fu, J. Zhang, and B. Luk'yanchuk, Magnetic light, *Sci. Rep.* **2**, 492 (2012).

¹² D. Smirnova and Y. S. Kivshar, Multipolar nonlinear nanophotonics, *Optica* **3**, 1241 (2016).

¹³ J. D. Jackson, *Classical Electrodynamics* (Wiley, New York, 1998).

¹⁴ E. M. Purcell and C. R. Pennypacker, Scattering and absorption of light by nonspherical dielectric grains, *The Astrophysical Journal* **186**, 705 (1973).

¹⁵ B. T. Draine, The discrete-dipole approximation and its application to interstellar graphite grains, *The Astrophysical Journal* **333**, 848 (1988).

¹⁶ M. A. Yurkin and A. G. Hoekstra, The discrete dipole approximation: An overview and recent developments, *J. Quant. Spectrosc. Radiat. Transfer* **106**, 558 (2007).

- ¹⁷ A. B. Evlyukhin, C. Reinhardt, and B. N. Chichkov, Multipole light scattering by nonspherical nanoparticles in the discrete dipole approximation, *Phys. Rev. B* **84**, 235429 (2011).
- ¹⁸ K. V. Baryshnikova, D. A. Smirnova, B. S. Luk'yanchuk, and Y. S. Kivshar, Optical Anapoles: Concepts and Applications, *Adv. Opt. Mater.* **7**, 1801350 (2019).
- ¹⁹ S. Raza, S. I. Bozhevolnyi, M. Wubs, and N. A. Mortensen, Nonlocal optical response in metallic nanostructures, *J. Phys.: Condens. Matter* **27**, 183204 (2015).
- ²⁰ C. David and F. J. G. de Abajo, Spatial Nonlocality in the Optical Response of Metal Nanoparticles, *J. Phys. Chem. C* **115**, 19470 (2011).
- ²¹ I. Fernandez-Corbaton, S. Nanz, R. Alaee, and C. Rockstuhl, Exact dipolar moments of a localized electric current distribution, *Opt. Express* **23**, 33044 (2015).
- ²² R. Alaee, C. Rockstuhl, and I. Fernandez-Corbaton, An electromagnetic multipole expansion beyond the long-wavelength approximation, *Opt. Commun.* **407**, 17 (2018).
- ²³ A. B. Evlyukhin, T. Fischer, C. Reinhardt, and B. N. Chichkov, Optical theorem and multipole scattering of light by arbitrarily shaped nanoparticles, *Phys. Rev. B* **94**, 205434 (2016).
- ²⁴ E. A. Gurvitz, K. S. Ladutenko, P. A. Dergachev, A. B. Evlyukhin, A. E. Miroshnichenko, and A. S. Shalin, The High-Order Toroidal Moments and Anapole States in All-Dielectric Photonics, *Laser Photonics Rev.* **13**, 1800266 (2019).
- ²⁵ L. D. Landau and E. M. Lifshitz, *Statistical Physics, Part 1* (Pergamon Press, Oxford, 1980).
- ²⁶ M. G. Silveirinha, Generalized Lorentz-Lorenz formulas for microstructured materials, *Phys. Rev. B* **76**, 245117 (2007).
- ²⁷ M. A. Gorlach and P. A. Belov, Effect of spatial dispersion on the topological transition in metamaterials, *Phys. Rev. B* **90**, 115136 (2014).
- ²⁸ A. V. Chebykin, M. A. Gorlach, and P. A. Belov, Spatial-dispersion-induced birefringence in metamaterials with cubic symmetry, *Phys. Rev. B* **92**, 045127 (2015).
- ²⁹ M. S. Dresselhaus, G. Dresselhaus, and A. Jorio, *Group Theory. Application to the Physics of Condensed Matter* (Springer, Berlin, 2008).